Jisha Joseph “Self-assembly of structurally diverse phosphomolybdates: synthesis, structure and properties.” Thesis. Research and Post gradute Department of Chemistry, St. Thomas college (autonomous), University of Calicut, 2020.

CHAPTER I

Introduction and Review of literature

Summary

Soft-chemistry routes provide favorable conditions for self-assembly of phosphomolybdates (PMOs) with peculiar properties. This chapter gives a brief outline on the various synthetic methodologies to design structurally diverse PMOs and major types of PMO cluster anions with their versatile structural features. Based on their self-assembly pattern they have been broadly classified into four distinct classes. Class I consists of PMO clusters covalently linked by transition metal complexes (TMCs) extending into multi-dimensions. Class II comprises of discrete PMO clusters with TMCs as counter cations. Class III includes PMO clusters derivatized by TMCs and Class IV comprises of coordination polymers in which PMO clusters have been incorporated. In addition, the important structural features of PMOs have been explained in a nutshell. PMOs have a wide range of applications, of which biomedicinal, catalytic, electrochemical and magnetic properties have been discussed.

I.1 Introduction

Polyoxometalates (POMs) are a prime class of oxo-bridged early transition metals in high oxidation states (such as Mo^{V}, Mo^{VI}, W^{VI}, V^{V}, Ta^{V} and Nb^{V}) [1,2]. These metal-oxygen anion clusters have contributed a lot towards the rapid development of inorganic chemistry in the past decades on account of their structural diversity and potential applications in fields of research such as medicine, catalysis, magnetism, photochemistry and redox chemistry [3-7]. The first POM, $\{PMo_{12}O_{40}\}^{3-}$ was reported by Berzelius in 1826 and later Keggin solved the structure of related anion $\{PW_{12}O_{40}\}^{3-}$ [8,9]. The POMs are broadly classified as isopolyanions with general formula of $\{M_nO_{(4n-m)}\}^{(2n-m)-}$ in which there are no heteroatoms present within the framework and heteropolyanions which include one or more heteroatoms within their frameworks with general formula of $\{X_xM_nO_m\}^{y-}$, where X= B^{III}, Si^{IV}, Ge^{IV}, P^{V}, $As^{III/V}$, Sb^{III}, Bi^{III}, Se^{IV} or Te^{IV} and M = V^{V}, Nb^{V}, Ta^{V}, Mo^{VI}, Mo^{V}, or W^{VI} (refer Scheme I.1).

Among the different heteropolyanion clusters, phosphorous and molybdenum containing clusters namely phosphomolybdates (PMOs) comprise of a distinguished family with versatile structural features and promising applications. The counter cations of phosphomolybdate anions can be (i) metal ions like Na^{+}, K^{+} Ca^{2+} and Cu^{2+} (ii) metal complexes and (iii) organic cations [10-15]. Formation of these types of crystalline solids is a self-assembly process. Being supramolecular materials, they can self-assemble into aggregates with multiple dimensionalities. There are a number of examples for 1-D, 2-D and 3-D networks of phosphomolybdates in the literature [16-18]. Intermolecular interactions like hydrogen bonding, π-π stacking and electrostatic interactions play a vital role in stabilizing the supramolecular assembly [19-21]. Although many researchers have been

exploring these solids, crystal engineering of PMO cluster anion based solids faces challenges including critical control of parameters such as pH and solubility of reactants. For example, Yan *et. al.* have explained the importance of pH of solution in the formation of PMO solids $(C_6H_{18}N_2)_2[H_2P_2Mo_5O_{23}].2H_2O$ and $(C_6H_{18}N_2)_{4.5}[H_3P_2Mo_5O_{23}].6H_2O$ which were synthesized using the same organic amine but at different pH levels [22]. Moreover, the crystallization of organic-inorganic hybrid PMO solids is a very complicated process due to unpredictable behavior of PMOs, metal ions and ligands during self-assembly which poses the problem of predicting the structure and composition of the final products [23]. Therefore, in the present work, a systematic synthesis of PMO cluster based solids was carried out using soft-chemistry routes to evaluate the role of parameters such as pH, nature of organic ligand and its concentration. Further, the structure elucidation of the synthesized solids was carried out and their properties were investigated.

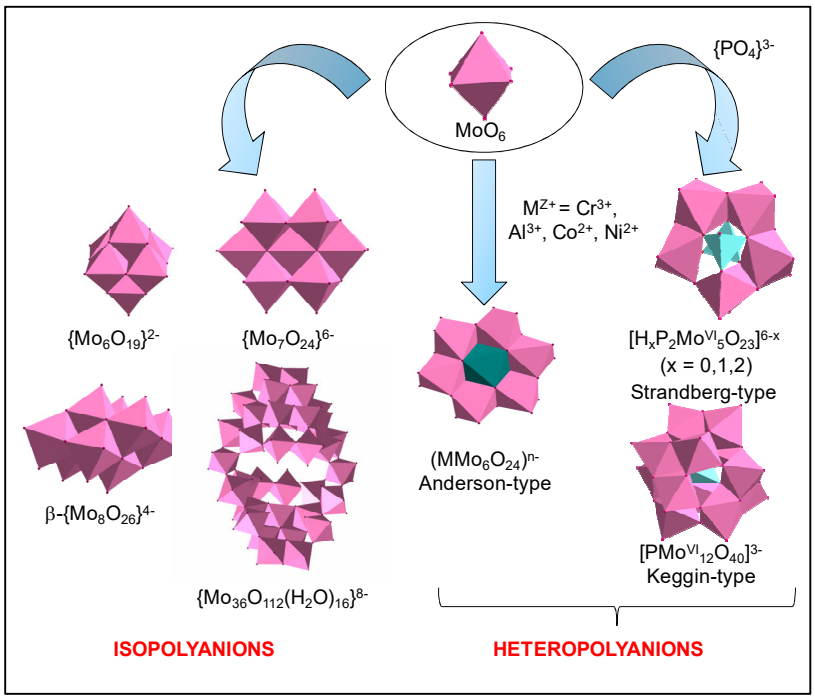

Scheme I.1. Scheme showing a few examples of isopolyanions and heteropolyanions of molybdenum.

I.2. Types of PMO clusters

POMs exhibit a large variety of clusters of varying sizes, shapes and composition. Based on their various topologies and intriguing frameworks different types of POM clusters have been reported in literature. Keggin, Anderson, Wells Dawson, Strandberg, and Silverton-type building blocks being the predominate ones in this area. Among these POMs, PMOs crystallize mainly as Strandberg-type $\{P_2Mo_5O_{23}\}^{6-}$, Keggin-type $\{PMo_{12}O_{40}\}^{3-}$, Wells Dawson-type $\{P_2Mo_{18}O_{62}\}^{6-}$ and as fully reduced cluster $\{P_4Mo_6O_{31}\}^{12-}$. Therefore, a brief discussion on the above mentioned cluster anions is given below.

I.2.1. Strandberg-type cluster $\{P_2Mo_5O_{23}\}^{6-}$

Diphosphopentamolybdate (VI) was first characterized by Strandberg in 1973 [24]. Relatively smaller size and higher electron density of the cluster anion favor the high coordination ability of the cluster anion. Strandberg-type of POMs are the first heteropolyanions in which organic groups are covalently bonded to a phosphorous heteroatom that allow a number of chemical reactions to take place in the intra-crystalline region [25]. As reported by Thomas *et. al.* $\{P_2Mo_5O_{23}\}^{6-}$ (abbreviated as $\{P_2Mo_5\}$ hence forth) is composed of "five distorted MoO_6 octahedra with two capped PO_4 tetrahedra. A pentagonal ring is formed by five MoO_6 octahedra by sharing edges and corners, which in turn is connected to two PO_4 tetrahedra to each side of the ring sharing three oxygen atoms with different MoO_6 units" [26]. Phosphorous atoms share three oxo groups with Mo ring where one exhibits μ_2-bridging linking one Mo site and phosphorous; while the other two exhibit μ_3- bridging linking two Mo sites and phosphorous (as shown in Figure I.1). The Mo-O distance can be divided into three distinct types: (i) short Mo-O terminal bonds of distance

1.689(3)-1.717(3)Å (ii) medium Mo-O bonds which link two Mo atoms of distance 1.897(3)-1.963(3)Å (iii) longer Mo-O bonds which link Mo and P atoms of distance 2.199(3)-2.417(4) Å [22,27]. This type of cluster forms reasonably stable anions in aqueous solution when a soluble molybdate source is acidified with phosphoric acid over a wide range of pH [28]. $[H_xP_2Mo_5O_{23}]^{(6-x)-}$ (x = 0,1,2) has been considered as an anionic building unit in the supramolecular assembly. The two extrusive $\{PO_4\}^{3-}$ groups enable coordination to bridging units and help in extending dimensionality [29]. The phosphorous heteroatom in Strandberg cluster can be inorganic phosphorous or organophosphine. Till date, several Strandberg-type POMs based on organophosphine $\{RPO_3H_2\}$ where R = $-C_6H_4CO_2H$, $-(CH_2)_nPO_3H_2$ (n = 2-6,9), $-(CH_2)_nCO_2H$ (n = 1,2), $-C_6H_5$, $-CH_2CH_3$, $-CH_3$ have been reported [30-32].

I.2.2. Keggin-type cluster $\{PMo_{12}O_{40}\}^{3-}$

Classical Keggin-type cluster anion (abbreviated as $\{PMo_{12}\}$ hence forth) consists of a central $\{PO_4\}$ tetrahedron surrounded by four vertex sharing $\{Mo_3O_{13}\}$ trimers which comprised of three $\{MoO_6\}$ octahedras linked in a triangular arrangement by sharing edges. The entire unit takes on a close-knit cage-type arrangement and is known as α-Keggin structure. By rotating one, two, three or all the four (Mo_3O_{13}) groups by 60° around the C_3 axis, stereoisomers (β-, γ-, δ- and ε- respectively) can be obtained [33]. Among these isomers, the α-isomer is the one which is widely studied structure with a stable framework (Figure I.2). The P-O bond lengths are in the range of 1.471(15)-1.609(16) Å. Mo-Ot (terminal), Mo-Oc (central) and Mo-Ob (bridge) bond lengths are in the ranges 1.646(5)-1.667(5) Å, 2.405(7)-2.518(7) Å, and 1.900(6)-1.993(6) Å respectively [34].

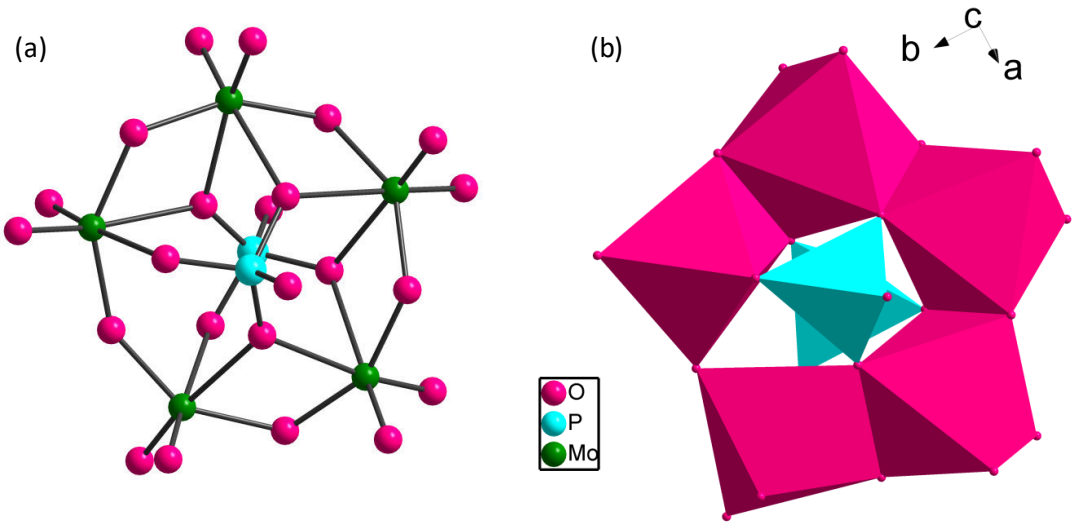

Figure I.1. (a) Ball-and-stick (b) polyhedral view of Strandberg-type anion.

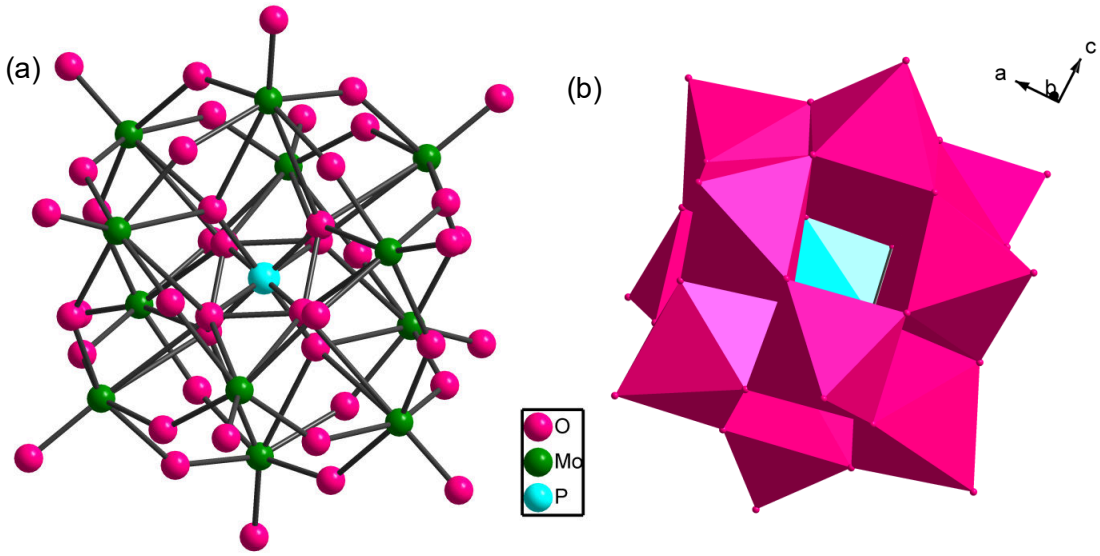

Figure I.2. (a) Ball-and-stick (b) polyhedral view of α-Keggin anion.

I.2.3. Wells Dawson-type cluster $\{P_2Mo_{18}O_{62}\}^{6-}$

Wells Dawson-type polyanion consists of 18 terminal and 36 μ_2-bridging oxygen atoms. There are eighteen MoO_6 octahedras present which exhibits two distinct structural types; six 'cap octhedras' which are divided into subsets of three and twelve 'belt octahedras' grouped

into two subsets of six as shown in Figure I.3 [35]. Six possible isomers are identified in Dawson structure, α, β, γ, α*, β* and γ*. The β isomer is obtained as result of rotation around the symmetry axis C_3 of the α structure by π/3. The symmetry of the molecule is lost and the Dawson structure is divided into two equivalent parts and attains a C_{3v} symmetry. The isomer γ is obtained by the second rotation of α isomer, around the symmetry axis C_3 by π/3 which leads to the symmetry plane. The isomers α*, β* and γ* are formed by the similar rotations of α, β and γ in the presence of an inversion centre [36].

I.2.4. Fully reduced cluster $\{P_4Mo_6O_{31}\}^{12-}$

In $\{P_4Mo_6O_{31}\}^{12-}$ (abbreviated as $\{P_4Mo_6\}$ hence forth) cluster anion, all the six Mo atoms are in +5 oxidation state. Six edge sharing MoO_6 octahedras form a ring decorated by four PO_4 tetrahedra. Three such tetrahedras are present in the ring and the fourth one at the midpoint. The central PO_4 tetrahedron furnishes three μ_3- O bridging the six molybdenum atoms; while the three peripheral PO_4 groups connect two molybdenum atoms by two oxygen atoms. In the presence of suitable organic ligands and at high temperature under hydrothermal conditions $\{P_4Mo_6\}$ forms as a competitive phase with $\{P_2Mo_5\}$ [37]. All the Mo(VI) ions which are in d^0 electronic configurations are transferred into d^1 Mo(V) ions. Unlike $\{P_2Mo_5\}$, fully reduced type PMOs requires a suitable metal ion (Fe^{2+}, Zn^{2+}, Mn^{2+}, Co^{2+}, Ni^{2+}, Cd^{2+}, Cu^{2+} and Na^+) for further stabilization [38] and the entire structure attains an hourglass-type dimer $\{M(P_4Mo_6O_{31})_2\}$ (refer Figure I.4).

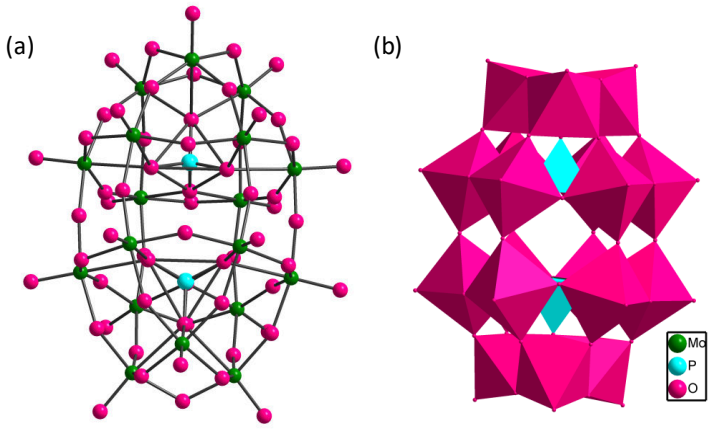

Figure I.3. (a) Ball-and-stick (b) polyhedral view of Wells Dawson-type anion.

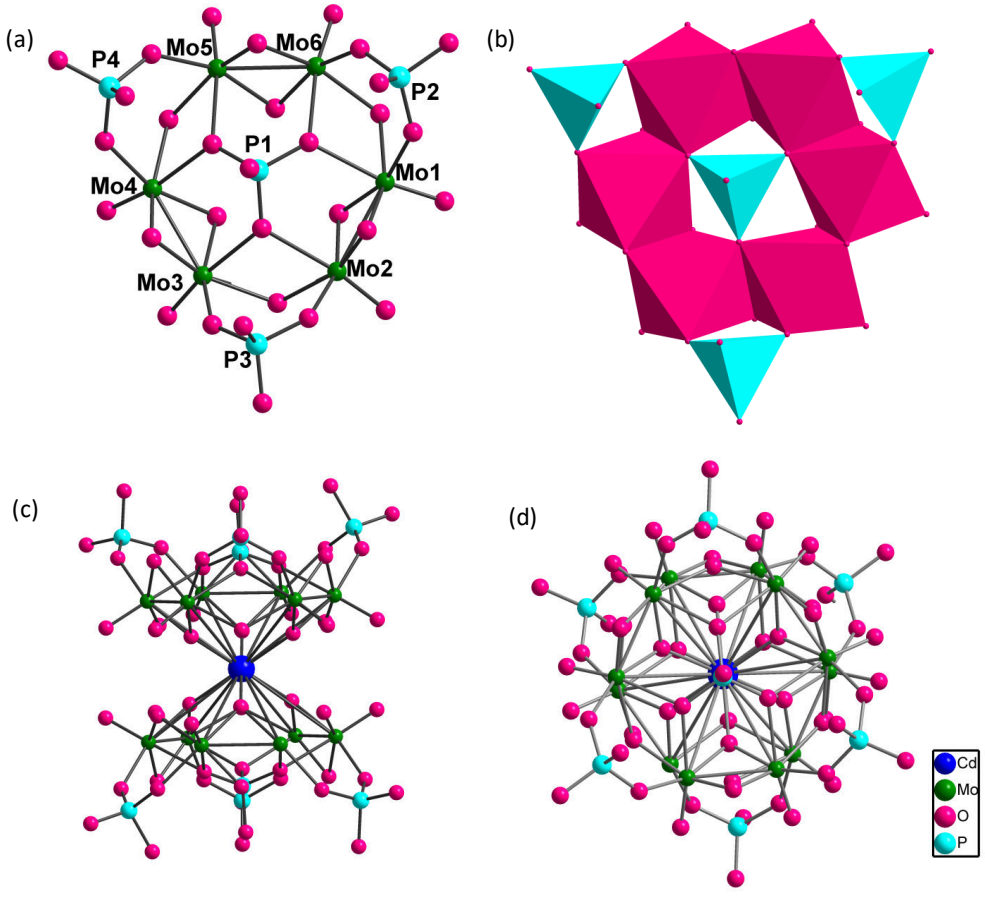

Figure I.4. (a) Ball-and-stick representation of top view of basic structural unit of $\{P_4Mo_6O_{31}\}^{12-}$ (b) polyhedral view of $\{P_4Mo_6O_{31}\}^{12-}$. (c) Side view and (d) top view of hourglass-type $\{M(P_4Mo_6O_{31})_2\}$.

I.3. Classification of PMO cluster based solids

The self-assembly of the basic structural unit PMO, organic ligands, metal ion and/or metal complex results in structural diversity including zero dimensional (0-D) species, one dimensional (1-D) chain, two dimensional (2-D) layer and three dimensional (3-D) framework. On the basis of their self-assembly pattern, PMO cluster based solids can be broadly classified as follows.

Class I: Solids in which PMO clusters are covalently linked to transition metal complexes (TMCs) extending into multi-dimensions.

Class II: Solids having discrete PMO clusters with TMCs as counter cations.

Class III: Solids in which PMO clusters are derivatized by TMCs to form either discrete or extended structures.

Class IV: Coordination polymers incorporated PMOs.

A brief explanation about each class is given below.

I.3.1. Class I

In this class the PMO cluster anion is covalently linked to TMCs extending the dimensionality into 1-D chains, 2-D sheets or 3-D frameworks. Strandberg-type cluster $\{P_2Mo_5O_{23}\}^{6-}$ contribute substantial amount of structures to this class as compared to other cluster anions. Class I solids reported in the literature during the last decade with TMCs of Ni^{2+}, Co^{2+}, Cu^{2+} and Zn^{2+} have been summarized in Table I.1. One of the examples of Class I solids is discussed herein. $[H_3O]_2[Cu_2(Pyim)_2(H_2O)_3][P_2Mo_5O_{23}].6H_2O$ (where *Pyim* = 2-(2′-pyridyl)-imidazole) reported by Hu *et. al.* [39] was synthesized under hydrothermal condition. The structure consists of $\{P_2Mo_5O_{23}\}^{6-}$ anion, two Cu^{2+} ions with different

coordination modes, two *Pyim* ligands, three coordinated water molecules and eight lattice water molecules. Cu(1) ion is five coordinated by two O atoms from two $\{P_2Mo_5O_{23}\}^{6-}$ clusters, two N atoms from one *Pyim* ligand and one O atom from a coordinated water molecule. The Cu(2) ion is six coordinated by two O atoms from two $\{P_2Mo_5O_{23}\}^{6-}$ anions, two N atoms from one *Pyim* ligand and two O atoms from two coordinated water molecules. It is interesting that each $\{P_2Mo_5O_{23}\}^{6-}$ cluster as a tetradentate inorganic ligand, connected by two Cu(1) and two Cu(2) complexes to form a 1-D infinite chain (refer Figure I.5).

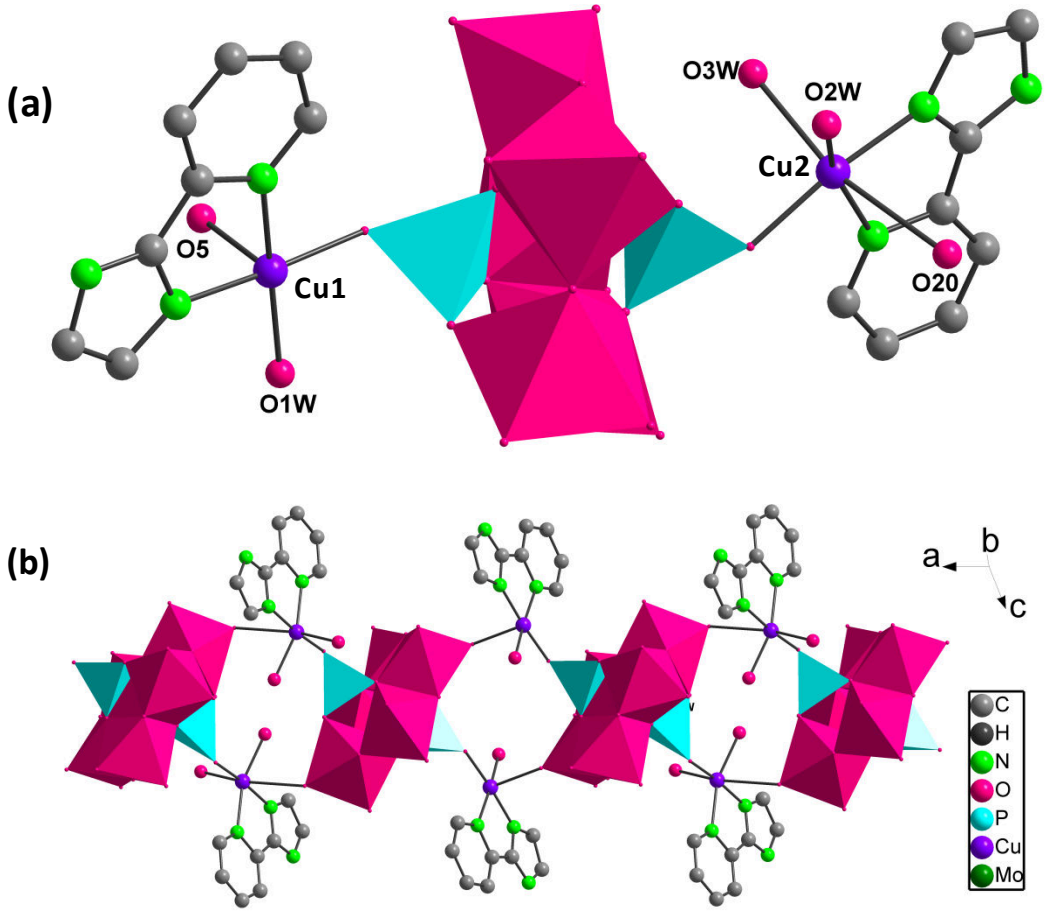

Figure I.5. (a) Figure showing coordination of $\{P_2Mo_5O_{23}\}^{6-}$ cluster anion with Cu(1) and Cu(2). (b) 1-D chain in $[H_3O]_2[Cu_2(Pyim)_2(H_2O)_3][P_2Mo_5O_{23}].6H_2O$. The hydrogen atoms and lattice water molecules have been removed for clarity.

Table I.1 Class I solids wherein PMO clusters are covalently linked to TMCs extending into multi-dimensions.

Sl No	Solid	Cluster	Structure description	Dimens-ionality	Ref.
1	$(pz)_2[\{Co(pz)_4\}_5\{P_2Mo_5O_{23}\}_2].6H_2O$ (*pz* = pyrazole)	$\{P_2Mo_5\}$	Two Co-Pyrazole complex units covalently link $\{P_2Mo_5\}$ clusters to form 2-D sheets and the third Co-*pz* complex unit connects the sheet to form a double sheet	2-D	[26]
2	$(pz)\{Ni(pz)_4(H_2O)_2\}[\{Ni(pz)_4\}_5\{P_2Mo_5O_{23}\}_2].2H_2O$ (*pz* = pyrazole)	$\{P_2Mo_5\}$	Two Ni-*pz* complex units covalently link $\{P_2Mo_5\}$ cluster into 2-D sheets and third Ni-*pz* complex unit connects the sheets to form a double sheet	2-D	[26]
3	$\{Cu(pz)_4(H_2O)_2\}[\{Cu(pz)_4\}\{Cu(pz)_4(H_2O)\}\{P_2Mo_5O_{23}\}].2H_2O$ (*pz* = pyrazole)	$\{P_2Mo_5\}$	Two asymmetric octahedral Cu-*pz* complexes link $\{P_2Mo_5\}$ clusters into a double chain which is capped by a third octahedral Cu-*pz* complex unit. A fourth complex unit occurs in between the chains as a counter cation	2-D	[26]
4	$(pz)[\{Zn(pz)_3\}_3\{P_2Mo_5O_{23}\}].2H_2O$ (*pz* = pyrazole)	$\{P_2Mo_5\}$	$\{P_2Mo_5\}$ cluster is linked to four trigonal pyramidal Zn units $\{Zn(py)_3O_2\}$ and one tetrahedral $\{Zn(py)_3O\}$ unit to form a 3-D framework	3-D	[26]
5	$Na_8[\{Cu(H_2O)_4\}(HP_2Mo_5O_{23})_2].8H_2O$	$\{P_2Mo_5\}$	$[P_2Mo_5O_{23}]^{6-}$ cluster is connected by $\{Cu(H_2O)_4\}$ linkers to form 1-D wave-like chain	1-D	[29]
6	$Na_8[\{Co(H_2O)_4\}(HP_2Mo_5O_{23})_2].6H_2O$	$\{P_2Mo_5\}$	$[P_2Mo_5O_{23}]^{6-}$ cluster is connected by $\{Co(H_2O)_4\}$ linkers to form 1-D wave-like chain	1-D	[29]
7	$[H_3O]_2[Cu_2(Pyim)_2(H_2O)_3][P_2Mo_5O_{23}].6H_2O$ (*Pyim* = 2-(2′-pyridyl)-imidazole)	$\{P_2Mo_5\}$	$\{P_2Mo_5O_{23}\}^{6-}$ clusters connected by copper complexes to generate one dimensional chain	1-D	[39]
8	$[Cu_3(Pyim)_3(H_2O)_4]$	$\{P_2Mo_5\}$	$\{P_2Mo_5O_{23}\}^{6-}$ clusters	1-D	[39]

	$[P_2Mo_5O_{23}]$.$7H_2O$ (*Pyim* = 2-(2′-pyridyl)-imidazole)		connected by copper complexes to generate one dimensional chain		
9	(H*imi*)[{Cu(*imi*)$_4$}$_2$ ($HP_2Mo_5O_{23}$)].$3H_2O$ (*imi* = imidazole)	{P_2Mo_5}	Cu-O coordination mediates the formation of a 2D sheet with $(H imi)^+$ and water molecules in the cavities of the 2-D sheet	2-D	[40]
10	[{Cu(*pz*)$_4$}$_2$ {$H_2P_2Mo_5O_{23}$}].H_2O (*pz* = pyrazole)	{P_2Mo_5}	{P_2Mo_5} clusters with copper pyrazole complex to give a 3-D framework	3-D	[40]
11	H_2[{Cu(H*L*)(H_2O)}$_2$ ($P_2Mo_5O_{23}$)].$5H_2O$ (H*L* = 2-acetylpyrazine thiosemicarbazone)	{P_2Mo_5}	Each Cu(II) is coordinated by one S atom and two N atoms of the ligand, O atom of the water molecule and one O_t atom of the cluster anion	3-D	[41]
12	$(C_5H_7N_2)_6$[Cu(H_2O)$_3$ $HP_2Mo_5O_{23}$]$_2$.$4H_2O$ (2-aminopyridine)	{P_2Mo_5}	Two bridging Cu(II) atoms link two adjacent P_2Mo_5 polyanions to give a centrosymmetric dimer $Cu_2(P_2Mo_5)_2$. The cluster is stabilized by O-H…O bonding	3-D	[42]
13	[Cu(*bim*)$_2$]$_2${[Cu(*bim*)$_2$]$_2$ [$PMo_9Mo_3O_{40}$]} (*bim* = benzimidazole)	{PMo_{12}}	The reduced Keggin PMo_{12} cluster is covalently bonded to two capping $[Cu^{II}(bim)_2]^{2+}$ fragments via its eight surface bridging oxygen atoms on two {Mo_4O_4} faces or pits in the opposite positions	3-D	[43]
14	[Cu(*mim*)$_2$]$_4$[$PMo_{11}MoO_{40}$]. H_2O (*mim* = 2-methylimidazole)	{PMo_{12}}	Every $[Cu^{I}(mim)_2]_4$ $[PMo^{VI}_{11}Mo^{V}O_{40}]$ unit is connected with four adjacent ones to form a tetrahedral structure	3-D	[43]
15	[Cu(*en*)(*en*H)]$_2$[$P_2Mo_5O_{23}$]. $3H_2O$ (*en* =ethylenediamine)	{P_2Mo_5}	Each $[P_2Mo_5O_{23}]^{6-}$ subunit is linked with adjacent four same subunits by four $[Cu(en)(enH)]^{3+}$ bridges	2-D	[44]
16	(H_2en_6){[$Zn(H_2O)_4$] ($P_2Mo_5O_{23}$)}$_3$.$10H_2O$ (*en* = ethanediamine)	{P_2Mo_5}	$[Zn(H_2O)_4]^{2+}$ connects adjacent $[P_2Mo_5O_{23}]^{6-}$ clusters to form 1-D chain	1-D	[45]
17	(H_2en)[Cu(*en*)(H_2O)	{P_2Mo_5}	Dinuclear Cu clusters	1-D	[46]

	$Cu(en)(H_2O)_3][P_2Mo_5O_{23}].5.5H_2O$ (*en* = ethanediamine)		alternate with $[P_2Mo_5O_{23}]^{6-}$ clusters in 1-D chains		
18	$(NH_4)_{2n}$ $\{[Cu(en)_2][Cu(en)(H_2O)][P_2Mo_5O_{23}]\}_n.3nH_2O$ (*en* = ethanediamine)	$\{P_2Mo_5\}$	The two different copper(II) fragments are connected to $[P_2Mo_5O_{23}]^{6-}$ clusters to form a 12-membered macrocycle. Cu(1) fragment is coordinated to the two phosphate oxygen atoms, and Cu(2) centre is bound to the 2 molybdenum oxygen atoms	1-D	[47]
19	$(NH_4)_{4n}\{[Cu(en)(H_2O)][P_2Mo_5O_{23}]\}_n.3.5nH_2O$ (*en* = ethylenediamine)	$\{P_2Mo_5\}$	1-D chains which is constructed from $[P_2Mo_5O_{23}]$ clusters linked through $[Cu(en)(H_2O)]$ subunits	1-D	[47]
20	$[\{Cu(H_2biim)(H_2O)\}_2$ $\{\mu$ -$Cu(H_2biim)(H_2O)\}$ $(P_2Mo_5O_{23})].20H_2O$ (*biim* = 2,2' – biimidazole)	$\{P_2Mo_5\}$	Two tetra-supporting heteropolyoxoanions linked via two Cu(II) complex fragments	3-D	[48]
21	$[Cu(H_2biim)_2(H_2O)]$ $[Cu(H_2biim)_2(HPO_4)_2$ $(Mo_5O_{15})].6H_2O$	$\{P_2Mo_5\}$	Constructed from a $[Cu(H_2biim)_2(H_2P_2Mo_5O_{23})]^{2-}$ polyoxoanion and a $[Cu(H_2biim)_2(H_2O)]^{2+}$ cation	3-D	[48]
22	$[H_2dahex]_4[Zn(H_2O)]_2\{Zn$ $[Mo_6O_{12}(OH)_3(HPO_4)_2$ $(PO_4)_2]_2\}.6H_2O$ (*dahex* = 1,6-diaminylhexane)	$\{P_4Mo_6\}$	$Zn[P_4Mo_6]_2$ clusters are linked by transition metal ions	3-D	[49]
23	$(H_2en)_3(H_2enme)_4(H_3O)$ $\{Cu[Mo_6O_{12}(OH)_3$ $(HPO_4)(PO_4)_3]_2\}.6H_2O$ (*en* = ethylene diamine *enme* = 1,2-diaminopropane)	$\{P_4Mo_6\}$	Cu bridges two $[P_4Mo_6]$ clusters by six μ_3-O to form a sandwich-type anion. Clusters are bridged through N-H…O bonds from PO_4 tetrahedra and protonated organic amines	3-D	[50]
24	$(H_2enme)_4\{Cu_2[Mo_6O_{12}$ $(OH)_3(PO_4)(HPO_4)_2$ $(H_2PO_4)]_2\}.3H_2O$ (*enme* = 1,2-diaminopropane)	$\{P_4Mo_6\}$	Two Cu atoms are in two coordination environments. Cu(1) is four coordinate by 2 oxygen atoms from two adjacent anion. Cu(2) bridges two$[P_4Mo_6]$ clusters via μ_3-O to form a	3-D	[50]

			sandwich-type anion		
25	$(L)_2[Co(H_2O)_4$ $P_2Mo_5O_{23}].6H_2O$ *L*= 3-(ammoniomethyl) pyridine	$\{P_2Mo_5\}$	$\{P_2Mo_5\}$ units linked by Co cations to form 1-D chain. The protonated ligands and the uncoordinated H_2O molecules connect adjacent chains into a 3-D supramolecular framework through hydrogen bonds	3-D	[51]
26	$[Ag_3(p\text{-}H_2pyttz)$ $(p\text{-}Hpyttz)Cl]$ $[H_2PMo_{12}O_{40}].6H_2O$ p-H_2pyttz = 3-(pyrid-4-yl)-5(1H-1,2,4-triazol-3-yl)-1,2,4-triazolyl)	$\{PMo_{12}\}$	PMo_{12} anions are the building blocks facilitating the extension of the framework. Three Ag^I ions are independent with three kinds of distinct coordination	3-D	[69]

I.3.2. Class II

In this class of solids, PMO cluster exists as a discrete moiety and the negative charges of the anion is compensated by TMC cations. In some cases, along with TMC ions, protonated organic moieties also contribute towards charge compensation. $\{P_2Mo_5\}$ and $\{P_4Mo_6\}$ type anions mainly constitute Class II solids. For example, the structure of $[Cu(L)_2(H_2O)_2]_2H_2[P_2Mo_5O_{23}].2CH_3OH$ (*L* = pyridine-2-carboxamide) described by Ji *et. al.* [14] consists of one $\{P_2Mo_5O_{23}\}^{6-}$, two $[Cu(L)_2(H_2O)_2]^{2+}$ and two methanol molecules. Two Cu(II) ions are in similar coordination environment, with six coordinated distorted geometry. Each Cu(II) ion is coordinated by two N atoms and two oxygen atoms from two ligands and with two oxygen atoms of water molecules. Four negative charges on the doubly protonated cluster anion were compensated by two $[Cu(L)_2(H_2O)_2]^{2+}$ complexes (Figure I.6). The limited examples of Class II solids reported in literature have been summarized in Table I.2.

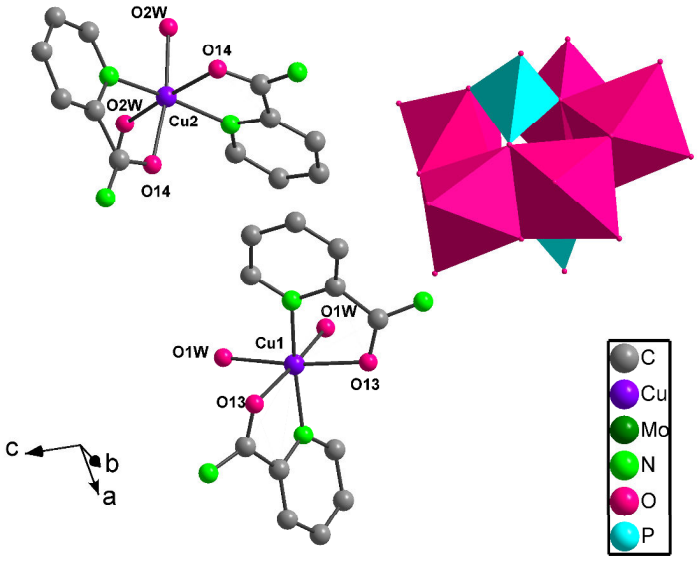

Figure I.6. Ball-and-stick and polyhedral representation of $[Cu(L)_2(H_2O)_2]_2H_2[P_2Mo_5O_{23}].2CH_3OH$ (L = pyridine-2-carboxamide). The hydrogen atoms and methanol molecules have been removed for clarity.

Table I.2. Class II solids having discrete PMO clusters with TMCs as counter cations

Sl No	Solid	Cluster	Structure description	Dimens-ionality	Ref.
1	$[Cu(L)_2(H_2O)_2]_2H_2[P_2Mo_5O_{23}].2CH_3OH$ (L = pyridine-2-carboxamide)	$\{P_2Mo_5\}$	Doubly protonated $[P_2Mo_5O_{23}]^{6-}$ is surrounded by two $[Cu(L)_2(H_2O)_2]^{2+}$ complex ions	Discrete cluster	[14]
2	$(H\mathit{imi})_6\{Cu(\mathit{imi})_2\}_2\{Cu(\mathit{imi})_2(H_2O)\}_2[Na\{(HPO_4)_4Mo_6(OH)_3O_{12}\}_2].7H_2O$	$\{P_4Mo_6\}$	The crystal packing is mediated by Na $\{P_4Mo_6O_{31}\}_2$, Cu(I) complex, $H\mathit{imi}^+$ moieties and lattice water molecules	Discrete cluster	[40]
3	$[Ni(HL)_2]_2H_2[P_2Mo_5O_{23}].4H_2O$ (L = 2-acetylpyridine-thiosemicarbazone)	$\{P_2Mo_5\}$	It consists of $[P_2Mo_5O_{23}]^{6-}$unit, two $[Ni(HL)_2]^{2+}$ cations, two protons and four lattice H_2O molecules	Discrete cluster	[52]
4	$[Co(L)_2(H_2O)_2]_2H_2[P_2Mo_5O_{23}]$.	$\{P_2Mo_5\}$	Doubly protonated	Discrete	[53]

	$2H_2O$ (*L* = pyridine-2-carboxamide)		$[P_2Mo_5O_{23}]^{6-}$ is surrounded by two $[Co(L)_2(H_2O)_2]^{2+}$ complex ions	cluster	
5	$\{(Nhep H_2)_2[Co(H_2O)_6]\}$ $[P_2Mo_5O_{23}].2H_2O$ *Nhep* = N-(2-hydroxyethyl)-piperazine	$\{P_2Mo_5\}$	$[P_2Mo_5O_{23}]^{6-}$ ion exists as a discrete moiety and the negative charges are compensated by both $[Co(H_2O)_6]^{2+}$ and $Nhep H_2^{2+}$	Discrete cluster	[54]

I.3.3. Class III

Class III consists of solids in which a metal ion may either substitute or cap the molybdenum centre. When one or more metal centers of classic PMO clusters are replaced by some transition metals (eg. Fe^{III}, Mn^{II}, Co^{II}, Ni^{II}, Zn^{II}) or any other element with similar properties (eg. W^{VI}, V^{V}), the resulting structure is known as 'lacunary' PMOs [55,56]. In this context, *Patel et. al*. have described the structure of $Cs_5[PCo(H_2O)Mo_{11}O_{39}].6H_2O$ in which, Co was distributed over the 12 positions and Co could not be distinguished from the 11 Mo's distributed equally over the 12 addenda atoms in the Keggin structure [57]. Although this feature can be considered as a disorder; it releases possibilities for a new range of applications, particularly, in catalysis [58]. In some cases, the cluster anions are connected through a common oxygen atom to the metal centre [59]. Mainly keggin-type PMOs are included in this class. There are only limited examples of derivatized $\{P_2Mo_5\}$ reported in the literature (refer Table I.3). In 2011, Jin *et. al.* have reported $Mg[Cu(bim)(H_2O)]_2[P_2Mo_5O_{23}].4H_2O$ wherein each $\{P_2Mo_5\}$ is decorated with $[Cu(bim)(H_2O)]^{2+}$ subunits (where *bim* = 2,2'-biimidazole) and the Mg atom which is positioned in between two $\{P_2Mo_5\}$ clusters interacting with six oxygen atoms of the cluster anion and is extended to a 1-D chain as shown in Figure I.7 [59].

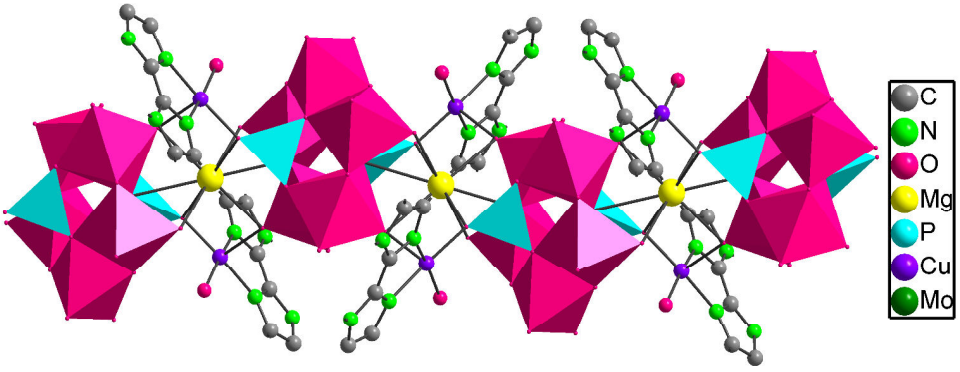

Figure I.7. 1-D chain of $Mg[Cu(bim)(H_2O)]_2[P_2Mo_5O_{23}].4H_2O$ which depicts the linkage of Mg^{2+} ion through the oxygen atoms of the $\{P_2Mo_5\}$cluster anion.

Table I.3. Class III solids in which PMO clusters derivatized by TMCs.

Sl No	Solid	Cluster	Structure description	Dimens-ionality	Ref.
1	$[Cu_4(tea)_6(H_4PMo_{11}CuO_{39})(PMo_{12}O_{40})]_2.33H_2O$ (*tea* =2-[1,2,4]triazol-4-yl-ethylamine)	$\{PMo_{11}Cu\}$	Consists of tetra-nuclear clusters $[Cu_4(tea)_6]$, linking a pair mono copper(II)-substituted and saturated Keggin anions	2-D	[13]
2	$[Cu_3(tea)_6(H_2O)_2(H_2PMo_{11}CuO_{39})_2]_2.30H_2O$ (*tea* =2-[1,2,4]triazol-4-yl-ethylamine)	$\{PMo_{11}Cu\}$	Contains tri-nuclear clusters $[Cu_3(tea)_6]$, fusing four mono copper(II) substituted anions	Discrete cluster	[13]
3	$(Himi)_3[\{Cu(imi)_3(H_2O)_2\}\{HP_2Mo_5O_{23}\}].3H_2O$	$\{P_2Mo_5\}$	The copper complex $\{Cu(imi)_3(H_2O)_3$ derivatizes the $\{P_2Mo_5\}$ cluster through Cu-O coordination to form $\{Cu(imi)_3(H_2O)_2\}\{HP_2Mo_5O_{23}\}$units	Discrete cluster	[40]
4	$(imi)(Himi)_2[\{Cu(imi)_2\}_2H_2P_2Mo_5O_{23}]$	$\{P_2Mo_5\}$	Cu(I) complex derivatizes the $\{P_2Mo_5\}$ cluster through Cu-O coordination. Oxygen atoms involved in derivatization belong to the same Mo centre	Discrete cluster	[40]

5	(*imi*)(H*imi*)$_2$[{Cu(*imi*)$_2$}$_2$ $H_2P_2Mo_5O_{23}$].H_2O	{P_2Mo_5}	Cu(I) complex derivatizes the {P_2Mo_5} cluster through Cu-O coordination. Oxygen atoms involved in derivatization belong to the neighboring Mo centre	Discrete cluster	[40]
6	$(C_5H_7N_2)_6$[Cu$(H_2O)_3$ $HP_2Mo_5O_{23}]_2$.4H_2O	{P_2Mo_5}	Two bridging Cu(II) atoms link two adjacent P_2Mo_5 polyanions to give a centrosymmetric dimer $Cu_2(P_2Mo_5)_2$	Discrete cluster	[42]
7	Cs_5[PCo$(H_2O)Mo_{11}O_{39}$]. 6H_2O	{$PMo_{11}Co$}	Transition metal Co and Mo atoms are distributed over 12 positions of Keggin cation	Discrete cluster	[57]
8	[Cu(H_2O)(*bim*)$_2$]{[Cu(H *bim*)$_2$][$P_2Mo_5O_{23}$]}.2H_2O *bim* = 2,2'-biimidazole	{P_2Mo_5}	Consists of one mono-supporting [Cu(H*bim*)$_2$] [$P_2Mo_5O_{23}$]}$^{2-}$ anion, one [Cu(H_2O)(*bim*)$_2$]$^{2+}$ counter ion and two lattice water molecules	Discrete cluster	[59]
9	[Cu(H*bim*)$_2$]{[Cu(*bim*) $(H_2O)_2]_2$[Cu(*bim*)$_2$]$_2$ [$(P_2Mo_5O_{23})_2$]}.20H_2O *bim* = 2,2'-biimidazole	{P_2Mo_5}	Consists of one [Cu(H*bim*)$_2$] cation and an isolated bi-supporting {[Cu(*bim*)$(H_2O)_2]_2$[Cu (*bim*)$_2]_2$[$(P_2Mo_5O_{23})_2$]}$^{4-}$ unit where the P_2Mo_5 cluster is supported by two distinct [Cu(*bim*)$(H_2O)_2$]$^{2+}$ and [Cu(*bim*)$_2$]$^{2+}$ fragments	Discrete cluster	[59]
10	[Cu(*phen*)(H_2O)][Cu (*bim*)$_2]_2$[$P_2Mo_5O_{23}$].H_2O *phen* =1,10-phenanthroline *bim* = 2,2'-biimidazole	{P_2Mo_5}	Consists of a tri-supporting [Cu(*phen*)(H_2O)] [Cu(*bim*)$_2]_2$[$P_2Mo_5O_{23}$] metal fragment and one lattice water molecule	Discrete cluster	[59]
11	Mg[Cu(*bim*)$(H_2O)]_2$ [$P_2Mo_5O_{23}$].4H_2O	{P_2Mo_5}	Consists of a Mg^{2+} cation, one {[Cu(*bim*) $(H_2O)]_2$[$P_2Mo_5O_{23}$]}$_2$ anion and four lattice water molecules. The neighboring {P_2Mo_5}	1-D	[59]

			clusters connect to each other via two $[Cu(bim)(H_2O)]^{2+}$ units and a Mg ion to form an unusual 1-D chain		
12	$[Cu(phen)(en)]$ $[Cu(phen)(en)(H_2O)]_2$ $[PMo_8Mo_4O_{40}$ $\{Cu(phen)\}_2]_2.6H_2O$ (*en* = ethylenediamine, *phen* = 1,10'-phenanthroline)	$\{PMo_{12}\}$	The reduced $[PMo_8Mo_4O_{40}]^{7-}$ is capped by two divalent Cu atoms through four bridging oxo groups on two opposite $\{Mo_4O_4\}$ faces	3-D	[60]
13	$[Cu(L)_2(H_2O)]H_2[Cu(L)_2$ $(P_2Mo_5O_{23})].4H_2O$ (*L* = pyridine-2-carboxamide)	$\{P_2Mo_5\}$	$(CuL_2)(P_2Mo_5O_{23})]^{6-}$ polyanion, $[CuL_2]^{2+}$ complex fragments and four water molecules	Discrete cluster	[61]
14	$[Cu(dmf)_6][PMo_{12}O_{40}$ $Cu(dmf)_4]$. *dmf* *dmf* = dimethyl formamide	$\{PMo_{12}\}$	Cu(1) interconnects two $[PMo^{V}Mo^{VI}_{11}O_{40}]^{4-}$ anion subunits and each $[PMo^{V}Mo^{VI}_{11}O_{40}]^{4-}$ polyoxoanion acts as a didentate ligand to link two Cu centers 1-D chain	1-D	[62]

I.3.4. Class IV

Class IV consists of solids in which organic ligands coordinated metal units are repeated and PMO clusters are incorporated within these metal-organic networks. Structure directing role of TMCs and multi-dentate ligands are equally important in the formation of coordination polymers [63-65]. Further, they can extend their dimensionality through H-bonding to form 2-D sheets and 3-D networks. For example, Hou *et. al.* have reported the formation 1-D chain in $[Cu_3$(4,4'-bis(pyrazol-1-ylmethyl)biphenyl)$_3][PMo_{12}O_{40}]$ (refer Figure I.8). In this solid, the bidentate ligands bridges Cu(I) ions to form 1-D cationic chain. The $\{PMo_{12}\}$ anion acts as a template, directing the $\{[Cu_3(L_2)_3]^{3+}\}$ coordination chains. Solids belonging to this type have been summarized in Table I.4.

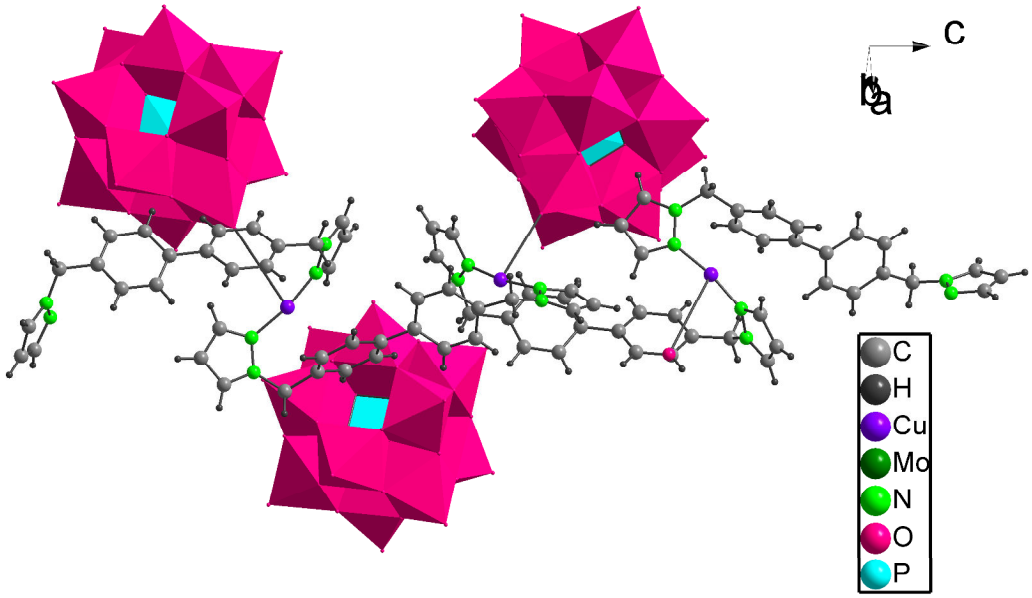

Figure I.8. 1-D chain formed in $[Cu_3(4,4'\text{-bis(pyrazol-1-ylmethyl)biphenyl})_3][PMo_{12}O_{40}]$

Table I.4. Class IV solids having coordination polymers incorporating PMOs.

Sl No	Solid	Cluster	Structure description	Dimens-ionality	Ref.
1	$(NH_4)_8[Co(bpy)_3]_2\{[Ca(H_2O)_3]_2[P_2Mo_5O_{23}]_3\}.21H_2O$ (*bpy* = 2,2'-bipyridine)	$\{P_2Mo_5\}$	Each Ca^{2+} cation is linked with three polyoxoanions, the formal $[Ca(P_2Mo_5O_{23})_{3/2}]$ subunits represent 3-connecting points forming a well-defined 3-D structure	3-D	[66]
2	$(NH_4)_5[Co(bpy)_3]\{[Ca(H_2O)_4]_2[Ca(H_2O)]_6[PMo_6O_{22}(PO_4)_3]_2\}.17H_2O$ (*bpy* = 2,2'-bipyridine)	$\{P_4Mo_6\}$	Ca^{2+} ions not only link polyoxoanions into the polymeric network but also connect phosphomolybdate clusters in dimers	3-D	[66]
3	$[Cu_3(L)_3][PMo_{12}O_{40}]$ *L* = 4,4'-bis(pyrazol-1-ylmethyl) biphenyl]	$\{PMo_{12}\}$	3-D supramolecular framework, which is formed by POM anions and $\{[Cu_3(L)_3]^{3+}\}_n$ cationic chains via hydrogen bonds	3-D	[67]
4	$[Cu_3(L)_4][PMo_{12}O_{40}]$	$\{PMo_{12}\}$	PMo_{12} cluster bridging	2-D	[67]

	[*L* = 1,4-bis (pyrazol-1-ylmethyl) benzene		the Cu^{I} ions to form infinite straight POM anion based chains. These chains graft onto the cationic skeletons by sharing the Cu1 ions giving rise to a POM containing a 2-D form		
5	$[Cu_3(bmtr)_3(PMo_{12}O_{40})]$ (*bmtr* = 1,3-bis(1-methyl-5-mercapto-1,2,3,4-tetrazole)propane)	$\{PMo_{12}\}$	$\{Cu_3(bmtr)_3\}$ forms a 1-D chain with $[PMo_{12}O_{40}]^{3-}$ polyanions and trinuclear clusters arranging alternately	1-D	[68]
6	$[Cu_6(m\text{-}pyttz)_2(H_2O)][HPMo_{12}O_{40}]$ (*m*-H_2pyttz = 3-(pyrid-3-yl)-5(1H-1,2,4-triazol-3-yl)-1,2,4-triazolyl)	$\{PMo_{12}\}$	*m-pyttz* ligands link Cu^{1} ions to generate 2-D layers	2-D	[69]

I.4. Structural features in PMO cluster based solids

Supramolecular self-assembly of PMOs consists of a basic building block which is the cluster anion. The secondary building units such as metal ions / metal complex, organic moieties and solvent molecules play a vital role in the construction of desired structures. Besides, factors like temperature, pH, molar ratio of metal and organic part are also vital for the supramolecular self-assembly [70]. A careful examination of the reported PMO structures show unique structural features particularly supramolecular isomerism, association of water clusters and porosity.

I.4.1. Supramolecular isomerism

According to Moulton and Zaworotko, “Supramolecular isomerism in this context is the existence of more than one type of network superstructure for the same molecular building blocks and is therefore related to structural isomerism at the molecular level. In other words,

the relationship between supramolecular isomerism and molecules is similar to that between molecules and atoms. In some instances, supramolecular isomerism can be a consequence of the effect of the same molecular components generating different *supramolecular synthons* and could be synonymous with polymorphism" [71]. In context of PMO cluster based solids, it can be explained using the following example. Thomas *et. al*. have reported two supramolecular isomers (*imi*)(H*imi*)$_2$[{Cu(*imi*)$_2$}$_2$H$_2$P$_2$Mo$_5$O$_{23}$] and (*imi*)(H*imi)*$_2$[{Cu(*imi*)$_2$}$_2$H$_2$P$_2$Mo$_5$O$_{23}$].H$_2$O [40] (Figure I.9). In both the isomers, Cu(I) complex derivatizes the {P$_2$Mo$_5$} cluster anion; but the manner of derivatization is different. In the first solid Cu^{I}-*imi* complex derivatizes {P$_2$Mo$_5$} cluster through oxygen atoms belonging to same Mo atom whereas in the second solid the derivatization occurs through oxygen atoms bonded to neighboring Mo atoms.

I.4.2. Aggregation of water clusters

Presence of water molecules in crystal structure provides dynamism in dimensionality and properties. The possibility of H-bonding increases the stability of the crystal packing. Occurrence of water clusters such as tetramers, pentamers and hexamers in metal–organic frameworks and the role of these water clusters in the supramolecular interactions have been reported in literature [72]. Thomas *et. al.* explained the crystal structure of (H*imi*)$_3$[{Cu(*imi*)$_3$(H$_2$O)$_2$} {HP$_2$Mo$_5$O$_{23}$}].3H$_2$O in which the decameric water cluster played a vital role in crystal packing of the solid (refer Figure I.10) [40].

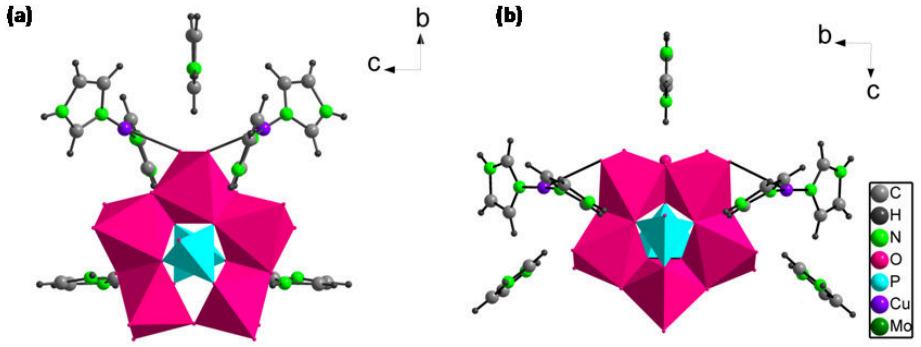

Figure I.9. Supramolecular isomerism exhibited by (a) (*imi*)(H*imi*)$_2$[{Cu(*imi*)$_2$}$_2$ $H_2P_2Mo_5O_{23}$].

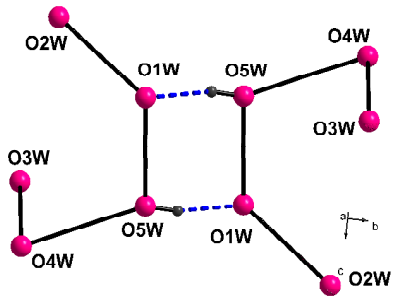

Figure I.10. Decameric water cluster in (H*imi*)$_3$[{Cu(*imi*)$_3$(H_2O)$_2$}{$HP_2Mo_5O_{23}$}].3H_2O.

1.4.3. Porosity

Usually POMs exhibit microporous or mesoporous behavior and extensive macroporosity has not been observed. Ammonium phosphomolybdate {NH_4}$_3$[$PMo_{12}O_{40}$].xH_2O, a Keggin-type PMO is a well studied example of porous PMOs [73-74]. The {PMo_{12}} cluster anions are linked by ammonium ions through H-bonding to form a 2-D sheet (refer Figure I.11). In 2011, Monge *et. al.* investigated the role of anions in ammonium salts used as precursor for the formation of ammonium phosphomolybdate. It was observed that the microporous / mesoporous pore size could be altered depending upon the anionic part in the ammonium salts. They tested the following salts: NH_4Cl, NH_4NO_3, $(NH_4)_2SO_4$, NH_4F, $NH_4CH_3CO_2$, $(NH_4)_2C_2O_4$, and $(NH_4)_2CO_3$ and found that nature of anion counter part of the ammonium

salt played a crucial role in the development of pore texture and pore size of microporous / mesoporous material [75]. On account of their porosity, PMOs are widely used as heterogeneous catalysts and adsorbents [76-78].

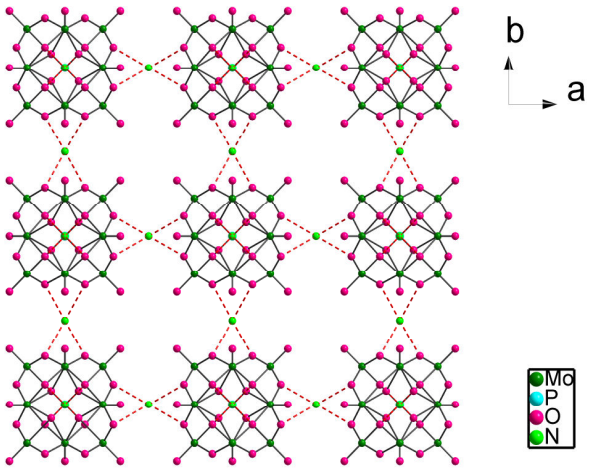

Figure I.11. $\{PMo_{12}\}$ clusters are linked by ammonium ions through H-bonding interaction (shown in dashed red lines) to form porous 2-D sheet in ammonium phosphomolybdate.

I.5. Synthetic strategies

In order to synthesize PMO cluster based solids mainly solvent evaporation technique and hydrothermal synthesis have been adopted in the present work. A brief explanation of each technique is given below.

I.5.1. Solvent evaporation technique

For the synthesis of $\{P_2Mo_5\}$ based solids, two different aqueous solutions with calculated molar ratio of $Na_2MoO_4.2H_2O$ (as the source of Mo) and metal chloride (to which organic ligand was added) were prepared. These two solutions are mixed while stirring and acidified with 1M H_3PO_4 (H_3PO_4 acts as the source of PO_4) and desired pH was adjusted with the same. The resultant solution was filtered in case of suspended particles and the clear solution

was kept undisturbed for crystallization in room temperature. The crystallized solids were filtered, washed with water and acetone and allowed to dry at room temperature.

I.5.2. Hydrothermal synthesis

One-pot hydrothermal synthesis is a commonly employed technique for the synthesis of PMOs. The reaction is carried out under autogenous pressure in a sealed Teflon container. All the precursors were added along with water. The reduced viscosity and iconicity of the solvent under high temperature and pressure conditions enhances the diffusion of the reactants and results in the self-assembly of the products. A temperature range from 100-250^{o}C can be used in a time span of 3-5 days. The slow cooling of the apparatus is allowed and product obtained was washed with water and acetone. The problem of low solubility of organic ligands in water can be resolved using this technique. A number of PMO based solids have been synthesized by hydrothermal method.

I.6. Applications of PMOs

PMOs on account of their tunable topology structures and reversible redox characteristics have found potential applications in various areas. The combination of metal-organic coordination with classical PMOs lead to a fascinating world of hybrid solids with potential magnetic, electronic, catalytical, optical, electrochemical and biological properties. Some dominant fields in which PMOs found remarkable applications are explained below.

I.6.1. Biomedicinal applications

The anticancer activity of PMOs were first reported in 1965, as the *in vivo* application of a mixture of $H_3[PW_{12}O_{40}]$, $H_3[PMo_{12}O_{40}]$ and caffeine, on patients suffering from

gastrointestinal cancer [79] and it was not subjected to further clinical studies. But today promising biological activities of PMOs are well documented in the literature; although the mechanism of action is still veiled. PMOs were found as potential inorganic drugs as anti-bacterial, anti-viral, anti-Alzheimer and anti-cancer agents [41,45,80]. It has been proposed that the therapeutic effects of some PMOs on cancerous cells are better than those of commercially available cancer drugs [41]. However, the cytotoxicity of PMOs on normal cells is a challenge. The biological properties of Strandberg-type PMOs are well established as compared to other cluster anions. Ji *et. al.* reported the effective *in vitro* activity of three {P_2Mo_5} based solids $[Cu(L)_2(H_2O)_2]_2$ $[H_2P_2Mo_5O_{23}].2CH_3OH$, $[Cu(L)_2(H_2O)][Cu(L)_2(H_2P_2Mo_5O_{23})].4H_2O$ and $[Cd(L)_2(H_2O)_2]_2$ $[H_2P_2Mo_5O_{23}].2CH_3OH$, (where *L* = pyridine-2-carboxamide) against HepG2 cells, HCT-116 cells and SMMC-7721 [81]. It is notable that both the coordination mode and the type of metal ion played important role in the cytotoxicity. $[Co(L)_2(H_2O)_2]_2[H_2P_2Mo_5O_{23}].2H_2O$ (where *L* = pyridine-2-carboxamide) disclosed potent activities against both HepG2 (human hepatocellular carcinoma) cells and HCT-116 (human colorectal cancer) cells and lower toxicity against normal HL-7702 (human normal hepatocyte) cells [53]. A nano-linear Zn-substituted $(H_2en)_6\{[Zn(H_2O)_4][P_2Mo_5O_{23}]\}_3.10H_2O$ (where *en* = ethanediamine) could inhibit the proliferation of *Escherichia coli (E. coli).* Zhao *et. al.* investigated the biological studies of $[\{Cu(HL)(H_2O)\}_2(H_2P_2Mo_5O_{23})].5H_2O$ (where *L*=2-acetylpyrazine thiosemicarbazone) and reported it's moderate antibacterial activity against *E. coli* and *Staphylococcus aureus* (*S. aureus*), and a better cytotoxicity against human hepatic cancer line (SMMC-7721) than Mitoxantrone , the current clinical anti-cancer drug [41]. In all the cases, researchers

mentioned that the synergistic effect of metal ion, organic moiety and the cluster anion was responsible for the biological activity.

On the other hand, there are studies which show that even without the presence of metal ion, the combination of organic ligands and PMO cluster alone can produce desirable results. For example, the *in vitro* anti-tumoral activity of the solid [{4,4'-H_2*bpy*}{4,4'-H*bpy*}$_2${$H_2P_2Mo_5O_{23}$}].5H_2O (where 4,4'-*bpy* = 4,4'-bipyridine) was tested against human breast cancer (MCF-7), human lung cancer (A549) and human liver cancer (HepG2) cells by Joshi *et. al.* and it was found that the solid showed anti-tumoral activity comparable to that of the commonly used chemotherapeutic agent Methotrexate [27]. [H*biz*]$_5$[$HMo_5P_2O_{23}$].5H_2O (where *biz*=benzimidazole) also showed *in vitro* anti-tumor activities against human neuroblastoma SHY5Y cells [82]. Advanced research is going on to develop PMO based next generation anti-tumor drugs which can selectively inhibit the affected cells while protecting the normal ones.

I.6.2. Applications in catalysis

PMOs have good catalytic properties by virtue of its super acidity and structural stability by which it can undergo multi-electron redox cycles. The catalytic behavior is remarkable both in activity and reusability. On account of the steric effect of the cluster based solids, they show regioselectivity and even enantioselectivity [83]. POM solids can also be used as both photocatalyst and electrocatalyst [84-87]. For example, three efficient and reusable catalysts for the protection of carbonyl compounds with glycol were reported by Li *et. al*. namely {H_4(H_2*biim*)$_3$}[Zn(H_2*biim*)(H_3*biim*)(H_2O)($HP_2Mo_5O_{23}$)]$_2$.3H_2O, {H_9(H_2*biim*)$_7$}[(μ-*biim*){($Zn(H_2O)_2)_{0.5}$($HP_2Mo_5O_{23}$)}$_2$].7H_2O and {H_7(H_2*biim*)$_7$}[Zn(H_2*biim*)(H_2O)$_2$($HP_2Mo_5O_{23}$)][$H_2P_2Mo_5O_{23}$].8H_2O (where *biim* = 2,2'-biimidazole) [88]. These are considered as the first

example where Strandberg-type PMOs are used as acid catalysts in an organic reaction. Paul *et. al.* synthesized two hybrid solids based on PMOs, $(NHEPH_2)_5$ $[Ni(P_4Mo_6O_{31})_2].6H_2O$ and $\{(NHEPH_2)_2[Co(H_2O)_6]\}[P_2Mo_5O_{23}].2H_2O$ (where *NHEP* = N-(2-hydroxyethyl)-piperazine) under hydrothermal conditions [54]. Both these solids were reported as excellent heterogeneous catalysts for the oxidation of styrene in the presence of an environmentally benign oxidant H_2O_2 under mild conditions to obtain benzaldehyde with more than 80% selectivity.

Solvent free green selective oxidation of alcohols catalysed by mono transition metal substituted Keggin-type $PMo_{11}M$ (M = Co, Mn, Ni) using hydrogen peroxide was reported by Pathan and co-workers with higher selectivity for the desired product [58]. Zhang *et. al.* tested the catalytic activity of three Keggin-type PMOs namely $(2\text{-}C_5H_7N_2)_4(PMo_{12}O_{40})_2(2\text{-}C_5H_6N_2)_6(C_4H_8N_4).H_2O$, $(3\text{-}C_5H_7N_2)_6(PMo_{12}O_{40})_2(3\text{-}C_5H_6N_2)_4H_8O_4(H_2O)_8$ and $(4\text{-}C_5H_7N_2)_6(PMo_{12}O_{40})_2(4\text{-}C_5H_6N_2)_4$ $(C_4H_6N_3)$ towards the oxidation of acetone [78]. The first and third solids were found to be more effective than the second one due to the different intensity and number of H-bonds which could be responsible for the adsorption ability of the reactants.

The most attractive group among PMOs in the area of catalysis are the fully reduced type $\{P_4Mo_6\}$, in which all the Mo atoms are in the reduced +5 valences. The reduced Mo^V centers of $\{P_4Mo_6\}$ exhibit d^1 electronic configuration, resulting a greater distribution of electronic density throughout the entire cluster. Moreover, they exist as hourglass-type structure where two half units of $[P_4Mo_6O_{31}]^{12-}$ are bridged in a centrally antisymmetric manner through a metal atom. A number of studies have been reported in literature on the effective reduction of hexavalent chromium, a highly toxic environmental pollutant [89-90].

Wang *et. al*. described the reduction of Cr^{VI} using three hybrid solids based upon hourglass-type $\{Mn[P_4Mo_6]_2\}$ units surrounded by protonated 1,3-bi(4-pyridyl)propane (abbreviated as *bpp*) ligands which are $(H_2bpp)_5[Na(Hbpp)]_6H_{10}\{Mn\ [Mo_6O_{12}\ (OH)_3(HPO_4)_4]_2\}_4.14H_2O$, $Na_4(H_2bpp)_2[Mn(H_2O)_7]\{Mn[Mo_6O_{12}(OH)_3(HPO_4)_3(PO_4)]_2\}.2H_2O$ and $Na(H_2O)_2(Hbpp)_3[Na_2(bpp)(H_2O)][Mn_2(H_2O)_5]\{Mn[Mo_{12}O_{24}(OH)_6(HPO_4)_6(H_2PO_4)(PO_4)]\}(HPO_4).H_2O$. Formic acid is used as the reducing agent and no secondary pollutants are formed during the process [37]. Compared to the traditionally used Pt/Pd nanoparticle catalyst these are less expensive and easy to prepare. Gong *et. al*. reported the same set of three $\{P_4Mo_6\}$ based PMOs as effective molecular catalysts for performing inorganic electron transfer reaction of ferricyanide to ferrocyanide by thiosulphate with high rate constants under mild conditions [84]. A series of Zn based $\{P_4Mo_6\}$ solids were reported as good photocatalysts for Cr^{VI} reduction on account of their wide visible-light absorption, suitable energy band structures and specific spatial arrangements of polyanionic species [91]. Recently, a few groups are developing composite materials based on PMOs such as sodium carboxymethyl cellulose – ammonium phosphomolybdate composites and phosphomolybdic acid – polyaniline – graphene composites as efficient and cost-effective heterogeneous catalysts [92].

I.6.3. Applications in magnetism

PMOs with electronic configurations other than d^0 like d^1 exhibit magnetic properties. Designing PMOs and their derivatives with unpaired electron system or with encapsulated small clusters of magnetic metal ions like Co(II) and nickel (II) can result in interesting magnetic behavior. According to Clemente-Juan *et. al*. PMOs have some advantages when compared to other coordination compounds. The robust POM molecule can keep their

integrity in solid state and in solutions. They can accommodate magnetic ions at the specific sites of their rigid structure leading to magnetic molecules [93]. By maintaining their structure they can accept electrons leading to a mixed valence system in which the extra electrons are widely delocalized over the framework. For example, Hu *et. al*. have reported two Strandberg-type PMOs $[H_3O]_2[Cu_2(Pyim)_2(H_2O)_3][P_2Mo_5O_{23}].6H_2O$ and $[Cu_3(Pyim)_3(H_2O)_4][P_2Mo_5O_{23}].7H_2O$ (where *Pyim* = 2-(2′-pyridyl)-imidazole) which exhibit antiferromagnetic interactions between copper ions [39].

I.6.4. Electrochemical applications

One of the fascinating properties of PMOs is their reversible multivalent reduction capability. Most of them have the ability to accept and release specific number of electrons without any change in their structural arrangement. However, PMOs face some challenges while they are used in electrocatalysis and other electrochemical applications. The main drawbacks are,

(i) low specific surface area

(ii) high water solubility

(iii) requirement of additional potential energy to increase the rate of electrochemical reactions

(iv) lack of selectivity and

(v) possible precipitation or adsorption of some PMO species on the substrate that may interfere with the measurements [94].

These problems can be solved by dispersing or immobilizing PMOs on various supports like polymers, nanoparticles, silica and carbon materials to enhance the number of active sites and to improve their electrochemical properties. In literature, a number of PMO based

composite materials based on Keggin-type PMO_{12} have been reported (discussed in Chapter VI). They can undergo multi-electron reversible redox processes. So, they have been exploited in a broad range of electrochemical applications such as electrocatalysts, energy storage systems and sensors. For example, Attapulgite/polyaniline/phosphomolybdic acid-based modified electrodes were used for the electrochemical determination of iodate [95]. The method showed advantages like good reproducibility, fast amperometric response and rapid preparation. Phosphomolybdic acid-polypyrrole/graphene composite modified glassy carbon electrode has been fabricated by Wang *et. al.* for the sensitive determination of folic acid based on the inhibitory activity of folic acid on account of the redox behavior of Keggin-type phosphomolybdic acid [96]. Papagianni *et. al*. introduced PMo_{12}-polyaniline composite as an electrochemical sensor for the determination of BrO_3^- ions [97]. On the contrary, the electrochemical properties of only few Strandberg-type PMOs have been investigated. For example, Wang *et. al.* reported three electrocatalysts $Na_{10}[Ag(P_2Mo_5O_{23})]_2.8H_2O$, $Na_8[\{Cu(H_2O)_4(HP_2Mo_5O_{23})_2].8H_2O$ and $Na_8[\{Co(H_2O)_4\}(HP_2Mo_5O_{23})_2].6H_2O$ for the reduction of hydrogen peroxide [29].

I.7. Motivation for the present study

PMOs are an important subclass of polyoxometalates with multi-faceted structures and distinctive properties. It is evident from literature that the area of PMOs is growing fast due to its promising applications. In this context, exploring the synthesis, characterization and investigation of properties of structurally diverse PMOs is an emergent area of interest. The self-assembly process of PMOs facilitates the incorporation of TMCs and organic cations during the aggregation of molecular precursors. Moreover, the properties of the solids can vary with the size and type of organic ligands; and the coordination complexes incorporated.

Transition metal containing molybdates are potential solids due to enhanced catalytic activity especially as oxidative catalysts. Incorporating TMCs can result in various solids ranging from discrete clusters to 3-D architectures. The ability to exhibit variable oxidation states enables the metal centers to exhibit different coordination preferences. In addition, TMCs are capable of exhibiting supramolecular interactions such as hydrogen bonding, CH…π and π…π stacking which influence the self-assembly of various architectures. Besides, TMCs based solids can also function as model systems to explore magnetic interactions such as localized spin interactions and can expand its application in the area of magnetism. Therefore based on the above observations, the major objectives of the thesis are,

(i) Systematically investigate the effect of metal ion/complex, organic moiety and reaction condition (ambient or hydrothermal) in the formation of PMO cluster based solids.

(ii) Explore the role of supramolecular interactions particularly hydrogen bonding, CH…π and π...π stacking in crystal packing of the synthesized solids.

(iii) Investigate electrochemical and magnetic properties of amine and TMC incorporated PMO solids respectively.

(iv) Evaluate the effectiveness of various PMO based solids in removing dye-stuffs from contaminated fresh water sources.

(v) Synthesize ammonium phosphomolybdate / polymer composites and investigate the properties along with the efficiency towards the removal of Cr(VI) from its aqueous solution.

References

1. Pope, M. T.; Muller, A. *Angew. Chem. Ind. Ed. Engl*. **1991**, 30, 34-48.
2. Zheng, S. T.; Yang, G. Y. *Chem. Soc. Rev*. **2012**, 41, 7623-7646.
3. Zong, L.; Wu, H.; Lin, H.; Chen, Y. *Nano Res*. **2018**, 11, 4149-4168.
4. Streb, C. *Dalton Trans*. **2012**, 41, 1651-1659.
5. Zhang, J.; Huang, Y.; Li. G.; Wei, Y. *Coord. Chem. Rev*. **2019**, 378, 395-414.
6. Ma, P.; Hu, F.; Wang, J.; Niu, J. *Coord. Chem. Rev.* **2019**, 378, 281-309.
7. Jiao, Y. Q.; Zang, H. Y.; Wang, X. L.; Zhou, E, L.; Song, B. Q.; Wang, C. G.; Shao, K. Z.; Su, Z. M. *Chem. Commun*. **2015**, 51, 11313-11316.
8. Berzelius, J. J. *Annalen der physic*. **1826**, 83, 261-288.
9. Keggin, J. F. *Nature* **1933**, 131, 908-909.
10. Niu, J.; Ma, J.; Zhao, J.; Ma, P.; Wang, J. *Inorg. Chem. Commun*. **2011**, 14, 474-477.
11. Zhang, L.; Li, X.; Zhou, Y.; Wang, X. J. *Mol. Struct*. **2009**, 928, 59-66.
12. Yan, D.; Fu, J.; Zheng, L.; Zhang, Z.; Xu, Y.; Zhu, X.; Zhu, D. *CrystEngComm*. **2011**, 13, 5133-5141
13. Tian, A.; Ni, H.; Tian, Y.; Ji, X.; Liu, G.; Ying, J. *Inorg. Chem. Commun*. **2016**, 68, 50-55.
14. Ji, Y. M.; Fang, Y.; Han, P. P.; Li, M. X.; Chen, Q. Q.; Han, Q. X. *Inorg. Chem. Commun.* **2017**, 86, 22-25.
15. Peng, Z. S.; Huang, Y. L.; Lu, S. Z.; Tang, J. T.; Cai, T. J.; Deng, Q. *Synth. React. Inorg. Met.-Org. Nano-Metal Chem.* **2014**, 44, 376-382.
16. Hu, G.; Dong, Y.; He, X.; Miao, H.; Zhou, S.; Xu, Y. *Inorg. Chem. Commun*. **2015**, 60, 33-36.

17. Qi, M.; Yu, K.; Su, Z.; Wang, C.; Wang, C.; Zhou, B.; Zhu, C. *Inorg. Chim. Acta* **2013**, 400, 59-66.
18. Qi, M. L.; Yu, K.; Su, Z. H.; Wang, C. X.; Wang, C. M.; Zhou, B. B.; Zhu, C. C. *Dalton Trans.* **2013**, 42, 7586-7594.
19. Meng, F. X.; Lv, J. H.; Yu, K.; Zhang, M. L.; Wang, K. P.; Zhou, B. B. *New. J. Chem*. **2018**, 42, 19528-19536.
20. Fu, Y. H.; Chen, X. Y.; Yang, W.; Bai, Y.; Dang, D. B. *Mater. Lett*. **2015**, 155, 48-50.
21. Wang, X.; Peng, J.; Alimaje, K.; Zhang, Z.; Shi, Z. *Inorg. Chem. Commun*. **2013**, 36, 141-145.
22. Yan, D.; Zheng, L.; Zhang, Z.; Wang, C.; Yuan, Y.; Zhu, D.; Xu, Y. *J. Coord. Chem*. **2010**, 63, 4215-4225.
23. Ren, Y.; Wang, M.; Chen, X.; Yue, B.; He, H. *Materials* **2015**, 8, 1545-1567.
24. Strandberg, R. *Acta Chem. Scand*. **1973**, 27, 1004-1018.
25. Gao, G.; Hong, H, G.; Mallouk, T. E. *Acc. Chem. Res*. **1992**, 25, 420.
26. Thomas, J.; Ramanan, A. *Inorg. Chim. Acta* **2011**, 372, 243-249.
27. Joshi, A.; Gupta, R.; Singh, B.; Sharma, D.; Singh, M. *Dalton Trans*. **2020**, 49, 7069-7077.
28. Asnani, M.; Kumar, D.; Duraisamy, T.; Ramanan, A. *J. Chem. Sci.* **2012**, 124, 1275-1286.
29. Wang, C.; Shi, J.; Yu, K.; Zhou, B. B. B. *J. Coord. Chem*. **2018**, 71, 3970-3979.
30. Lu, T.; Feng, S. L.; Zhu, Z. M.; Sang, X. J.; Su, F.; Zhang, L. C. *J. Solid State Chem*. **2017**, 253, 52-57.

31. Sun, S.; Liu, X.; Yang, L.; Tan, H.; Wang, E. *Eur. J. Inorg. Chem*. **2016**, 2016, 4179-4184.

32. Feng, S. L.; Lu, Y.; Zhang, Y. X.; Su, F.; Sang, X. J.; Zhang, L. C.; You, W. S.; Zhu, Z. M. *Dalton Trans.* **2018**, 47, 14060-14069.

33. Li, D.; Ma, P.; Niu, J.; Wang, *J. Coord. Chem. Rev*. **2019**, 392, 49-80.

34. Han, Z.; Gao, Y.; Zhai, X.; Peng, J.; Tian, A.; Zhao, Y.; Hu, C. *Cryst. Growth Des*. **2009**, 9, 1225-1234.

35. Li, L.; Ma, P.; Wang, J.; Niu, J. *Inorg. Chem. Commun*. **2013**, 34, 23-26.

36. Amman, M. *J. Mater. Chem. A* **2013**, 1, 6291-6312.

37. Wang, X.; Wang, J.; Geng, Z.; Qian, Z.; Han, Z. *Dalton Trans.* **2017**, 46, 7917-7925.

38. Dong, Y.; Dong, Z.; Zhang, Z.; Liu, Y.; Cheng, W.; Miao, H.; He, X.; Xu, Y. *ACS Appl. Mater. Interfaces* **2017**, 27, 22088-22092.

39. Hu, G.; Dong, Y.; He, X.; Miao, H.; Zhou, S.; Xu, Y. *Inorg. Chem. Commun*. **2015**, 60, 33-36.

40. Thomas, J. ; Kumar, D. ; Ramanan, A. *Inorg. Chim. Acta* **2013**, 396, 126–135.

41. Zhao, H.; Li, J.; Fang, Y.; Chang, B.; Meng, Q.; Li, M.; Wang, C.; Zhu, X. *Bioorg. Med. Chem. Lett.* **2020**, 30, 126781-126786.

42. Ammari, Y.; Dhahri, E.; Rzaigui, M.; Hlil, E. K.; Abid, S. *J. Clust. Sci*. **2016**, 27, 1213-1227.

43. Hu, J. K.; Yu, X. Y.; Luo, Y. H.; Wang, X. F.; Yue, F. X.; Zhang, H.; *Inorg. Chem. Commun*. **2013**, 32, 37-41.

44. Zhao, W. J.; Li, Y. Y.; Wang, Y. H.; Shi, D. Y.; Luo, J.; Chen, L. J. *Russ. J. Coord. Chem*. **2013**, 39, 519-523.

45. Ma, X.; Zhou, F.; Yue, H.; Hua, J.; Ma, P. *J. Mol. Struct*. **2019**, 1198, 126865-126872.

46. Ma, X.; Zhang, C.; Hua, J.; Ma, P.; Wang, J.; Niu, J. *CrystEngComm.* **2019**, 21, 394-398.

47. Buvailo, H. I.; Makhankova, V. G.; Kokozay, V. N.; Zatovsky, I. V.; Omelchenko, I. V.; Shishkina, S. V.; Zabierowski, P.; Matoga, D.; Jezierska, J. *Eur. J. Inorg. Chem.* **2016**, 2016, 5456-5466.

48. Wang, Y. ; Zhang, L. C. ; Zhu, Z. M. ; Li, N. ; Deng, A. F. ; Zheng, S. Y. *Transition Met. Chem*. **2011**, 36, 261-267.

49. Xu, X.; Ju, W.; Yan, D.; Jian, N.; Xu, Y. *J. Coord. Chem*. **2013**, 66, 2669-2678.

50. Xu, X.; Yan, D.; Fan, X.; Xu, Y. *J. Coord. Chem*. **2012**, 65, 3674-3683.

51. Ammari, Y.; Baaalla, N.; Hlil, E.K. *Sci. Rep.* **2020**, 10, 1316-1328.

52. Li, J.; Zhao, H.; Ma, C.; Han, Q.; Li, M.; Liu, H. *Nanomaterials* **2019**, 9, 649.

53. Ji, Y. M.; Zhao, M.; Han, P. P.; Fang, Y.; Han, Q. X.; Li, M. X. *J. Inorg. Nano-Met. Chem*. **2018**, 48, 421-425.

54. Paul, L.; Dolai, M.; Panja, A.; Ali, M. *New J. Chem.* **2016**, 40, 6931-6938.

55. Patel, A.; Narkhede, N.; Singh, S.; Pathan, S. *Cat. Rev. - Sci. Eng*. **2016**, 58, 337-370.

56. Gaunt, A. J.; May, L.; Sarsfield, M. J.; Collison, D.; Helliwell, M.; Denniss, L. S. *Dalton Trans.* **2003**, 13, 2767-2771.

57. Patel, A.; Pathan, S. *J. Coord. Chem*. **2012**, 65, 3122-3132.

58. Pathan, S.; Patel, A. *Appl. Catal. A* **2013**, 459, 59-64.

59. Jin, H. J.; Zhou, B. B.; Yu, Y.; Zhao, Z. F.; Su, Z. H. *CrystEngComm* **2011**, 13, 585-590.

60. Ma, F. X.; Chen, Y. G.; Yang, H. Y.; Dong, X. W.; Jiang, H.; Wang, F.; Li, J. H. *J. Clust. Sci*. **2018**, 30, 123-129.

61. Fang, N.; Ji, Y. M.; Li, C. Y.; Wu, Y. Y.; Ma, C. G.; Liu, H. L.; Li, M. X. *RSC Adv.* **2017**, 7, 25325-25333.

62. Bai, Y.; Zheng, G. S.; Dang, D. B.; Gao, H.; Qi, Z. Y.; Niu, J. Y. *Spectrochim. Acta Part A* **2010**, 77, 727-731.

63. Jiang, K.; Ma, L. F.; Sun, X. Y.'; Wang, L. Y. *CrystEngComm* **2011**, 13, 330-338.

64. Song, X.; Zhu, W.; Yan, Y.; Gao, H.; Gao, W.; Zhang, W.; Jia, M. *Microporous Mesoporous Mater.* **2017**, 242, 9-17.

65. Batten, S. R.; Champness, N. R.; Chen, X. M.; Martinez, J. G.; Kitagawa, S.; Ohrstrom, L.; O'Keeffe, M.; Suh, M. P.; Reedijk, J. *Pure Appl. Chem*. **2013**, 85, 1715-1724.

66. Buvailo, H. I.; Makhankova, V. G.; Kokozay, V. N.; Omelchenko, I. V.; Shishkina, S. V.; Zabierowski, P.; Matoga, D.; Jezierska, J. *Eur. J. Inorg. Chem*. **2017**, 2017, 3525-3532.

67. Hou, G.; Bi, L.; Li, B.; Wu, L. *Inorg. Chem.* **2010**, 49, 6474-6483.

68. Wang, X. L.; Gao, Q.; Tian, A. X.; Hu, H. L.; Liu, G. C. *J. Solid State Chem*. **2012**, 187, 219-224.

69. Li, X.; Wang, Y.; Zhou, K.; Wang, Y.; Han, T.; Sha, J. *J. Coord. Chem*. **2018**, 71, 468-482.

70. Meng, J, X.; Lu, Y.; Li, Y. G.; Fu, H.; Wang, E. B. *CrystEngComm* **2011**, 7, 2479-2486.

71. Moulton, B.; Zaworotko, M. J. *Chem. Rev.* **2001**, 101, 1629-1658.

72. Upreti, S.; Datta, A.; Ramanan, A. *Cryst. Growth Des.* **2007**, 7, 966-971.

73. Kendell, S. M.; Alston, A. S.; Ballam, N. J.; Brown, T. C.; Burns, R. C. *Catal. Lett.* **2011**, 141, 374-390.

74. Ghalebi, H. R.; Aber, S.; Karimi, A. *J. Mol. Catal. A: Chem.***2016**, 415, 96-103.

75. Monge, J. L.; Trautwein, G.; Martinez, M. C. R. *Solid State Sci*. **2011**, 13, 30-37.

76. Chen, Q.; Shen, L. M.; Xia, J.; Chen, X. W.; Wang, J. H. *J. Sep. Sci.* **2014**, 37, 2716-2723.

77. Huynh, Q.; Schuurman, Y.; Delichere, P.; Loridant, S.; Millet, J. M. M. *J. Catal.* **2009**, 261, 166-176.

78. Zhang, C.; Shen, X.; Lu, S.; Peng, Z.; Zhu, W.; Cai, T. *J. Mol. Struct*. **2012**, 1016, 155-162.

79. Mukherjee, H. N. *J. Indian Med. Assoc*. **1965**, 44, 477-479.

80. Bijelic, A.; Aureliano, M.; Rompel, A. *Angew. Chem. Int. Ed*. **2019**, 58, 2980-2999.

81. Ji, Y. M.; Fang, Y.; Han, P. P.; Li, M. X.; Chen, Q. Q.; Han, Q. X. *Inorg. Chem. Commun.* **2017**, 86, 22-25.

82. Qu, X.; Feng, H.; Ma, C.; Yang, Y.; Yu, X. *Inorg. Chem. Commun*. **2017**, 81, 22-26.

83. Ren, Y.; Wang, M.; Chen, X.; Yue, B.; He, H. *Materials* **2015**, 8, 1545-1567.

84. Gong, K.; Liu, Y.; Han, Z. *RSC Adv*. **2015**, 5, 47004-47009.

85. Shi, S.; Chen, Y.; Zhao, X.; Ren, B.; Cui, X.; Zhang, J. *Inorg. Chim. Acta* **2018**, 482, 870-877.

86. Xu, M.; Li, F.; Wang, T.; Xu, L. *Inorg. Chem. Commun*. **2018**, 94, 123-126.

87. Wan, S.; Yu, K.; Wang, L.; Su, Z.; Zhou, B. *Inorg. Chem. Commun*. **2015**, 61, 113-117.

88. Li, Z. L.; Wang, Y.; Zhang, L. C.; Wang, J. P.; You, W. S.; Zhu, Z. M. *Dalton Trans*. **2014**, 43, 5840-5846.

89. Xin. X.; Tian, X.; Yu, H.; Han, Z. *Inorg. Chem.* **2018**, 57, 11474-11481.

90. Tian, X.; Hou, L.; Wang, J.; Xin, X.; Zhang, H.; Ma, Y.; Wang, Y.; Zhang, L.; Han, Z. *Dalton Trans*. **2018**, 47, 15121-15130.

91. Hou, L.; Zhang, Y.; Ma, Y.; wang, Y.; Hu, Z.; Gao, Y.; Han, Z. *Inorg. Chem.* **2019**, 58, 16667-16675.

92. Zhang, N.; Chen, S.; Hu, J.; Shi, J.; Guo, Y.; Deng, T. *RSC Adv*. **2020**, 10, 6139.

93. Juan, J. M. C.; Coronado, E.; Arino, A. G. *Chem. Soc. Rev*. **2012**, 41, 7464-7478.

94. Fernandes, D. M.; Freire, C. *ChemElectroChem* **2015**, 2, 269-279.

95. Zhang, S.; He, P.; Lei, W.; Zhang, G. *J. Electroanal. Chem.* **2014**, 724, 29-35.

96. Wang, Z.; Han, Q.; Xia, J.; Xia, L.; Bi, S.; Shi, G.; Zhang, F.; Xia, Y.; Li, Y.; Xia, L. *J. Electroanal. Chem.* **2014**, 726, 107-111.

97. Papagianni, G. G.; Stergiou, D. V.; Armatas, G. S.; Kanatzidis, M. G.; Prodromidis, M. I. *Sens. Actuators, B* **2012**, 173, 346-353.